International Journal of Pharmaceutics 677 (2025) 125650

Contents lists available at ScienceDirect

International Journal of Pharmaceutics

journal homepage: www.elsevier.com/locate/ijpharm

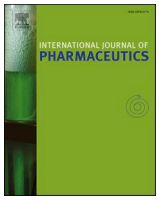

In-situ hyaluronic acid-tyramine hydrogels prolong the release of extracellular vesicles and enhance stability☆

Yingchang Ma, Ines Colic, Maha Muwaffak, Ahad A. Rahim, Steve Brocchini, Gareth R. Williams *

UCL School of Pharmacy, University College London, 29–39 Brunswick Square, London WC1N 1AX, UK

ARTICLE INFO

Keywords:
In-situ hydrogel
Extracellular vesicles
Controlled release

ABSTRACT

Hydrogels can provide a hydrated environment to encapsulate extracellular vesicles (EVs) while offering promising solutions to some of the challenges that limit their therapeutic potential, e.g. rapid clearance and propensity for enzymatic degradation and aggregation. This study explores the use of a hyaluronic acid-tyramine (HA-TA) hydrogel to prolong the delivery and enhance the stability of EVs. EVs were obtained from lentiviral-transduced HEK293T cells expressing luciferase and eGFP to enable easy quantification. Two encapsulation strategies were evaluated: (1) pre-loading, where EVs were mixed with HA-TA (2.58 % degree of substitution) precursor solution and subsequently crosslinked with 2 U/mL horseradish peroxidase (HRP) and 0.05 mM H_2O_2; and (2) post-loading, where EVs were soaked into pre-formed dehydrated hydrogels. Both methods improved EV stability over 7 days at 37 °C compared to free EVs. The pre-loading approach was ultimately selected due to its ability to give rapid *in situ* gelation within one minute. Controlled *in vitro* release of EVs from the pre-loaded hydrogels was observed to extend beyond 7 days, as determined by CD9 ELISA. The released EVs maintained their bioactivity, as evidenced by effective internalisation into ARPE-19 and H9c2 cell lines, with performance comparable to fresh EVs. The EV release profile could be varied by modifying the hydrogel concentration. These findings underscore the potential of HA-TA hydrogels for localised, sustained, EV delivery with preserved functionality.

1. Introduction

Extracellular vesicles (EVs) are particles with lipid bilayers naturally released by all cell types. They serve as key mediators of intercellular communication and tissue homeostasis (Simons and Raposo, 2009). By delivering a variety of cargos including proteins, lipids, and nucleic acids, EVs influence the behaviour and phenotype of target cells (Rackov et al., 2018; Simons and Raposo, 2009; Valadi et al., 2007). Additionally, EVs can transmit signalling molecules through surface-expressed ligands (Chen et al., 2021). Their inherent targeting capabilities and ability to cross membrane barriers, such as the blood brain barrier (BBB), have positioned EVs as promising therapeutic delivery systems (Das et al., 2019). As endogenous biological carriers, EVs offer superior compatibility with the immune system compared to synthetic nanocarriers, reducing the risk of immune responses and toxicity (Lu et al., 2018). Furthermore, mounting evidence suggests that the therapeutic effects of progenitor cell therapy are largely mediated by paracrine factors, particularly EVs, which often exhibit comparable or even superior therapeutic properties to their parent cells (Jung et al., 2017). Thus, EV therapies have emerged as a viable alternative to direct cell transplantation, offering benefits of avoiding immune rejection and eliminating the need for immunosuppressive treatments (Melling et al., 2019).

Free-form EVs can be administered via various routes, with intravenous injection being the most extensively studied. However, intravenously administered EVs are rapidly cleared from the circulation and tend to accumulate in the liver, kidneys, lungs, and spleen, limiting their distribution to other target tissues (Lai et al., 2014; Takahashi et al., 2013; Wiklander et al., 2015). As a result, high doses are often necessary to overcome this limited distribution, which may increase the risk of adverse effects *in vivo* (Wiklander et al., 2015). Local delivery of EVs, particularly via embedding them within biomaterials, has gained

☆ This article is part of a special issue entitled: 'Parenteral Time-Controlled Drug Delivery' published in International Journal of Pharmaceutics.

* Corresponding author.
E-mail address: g.williams@ucl.ac.uk (G.R. Williams).

https://doi.org/10.1016/j.ijpharm.2025.125650
Received 13 March 2025; Received in revised form 24 April 2025; Accepted 25 April 2025
Available online 29 April 2025

increasing interest. This approach allows for localised and concentrated EV delivery while minimising distribution to unwanted tissues. Using biomaterials as delivery vehicles can offer improved EV stability with prolonged therapeutic effect (Riau et al., 2019) and the potential for triggered release in response to environmental changes at the tissue site of release (Ma et al., 2023; Riau et al., 2019).

Hydrogels are promising biomaterials for localised EV delivery. These three-dimensional (3D) polymer networks, formed through covalent or non-covalent crosslinking (Deng et al., 2012; Lee, 2018), can absorb and retain substantial amounts of water, creating a hydrated environment well-suited for EV encapsulation (Li and Mooney, 2016). Hydrogels fabricated from natural polymers, particularly hyaluronic acid (HA), are widely recognised for their biocompatibility (Ju et al., 2023). HA is a natural glycosaminoglycan (GAG), a major component of the extracellular matrix (ECM), and is present in nearly all body tissues and fluids (Yasin et al., 2022). Its abundant hydroxyl groups enable hydrogen bonding with water molecules, enhancing hydrophilicity (Saranraj and Naidu, 2013). HA has been widely used in clinically approved applications, including dermal fillers, viscosupplements (Fakhari and Berkland, 2013), and ophthalmic formulations (Rah, 2011), due to its biocompatibility and viscoelasticity. To strengthen its mechanical properties and stability, HA chains can be crosslinked into hydrogels by modifying their reactive hydroxyl and carboxyl groups (Choi et al., 2019). For example, in load-bearing tissues such as the knee, crosslinked hydrogels (e.g. Gel-One®) are often used in injections, as they demonstrate longer persistence *in vivo* compared to non-crosslinked HA, which tends to diffuse rapidly post-injection (Strand et al., 2012).

Tyramine-modified HA (HA-TA) hydrogels have been reported for applications in protein delivery (Lee et al., 2009) and tissue engineering (Toh et al., 2012). HA-TA hydrogels may offer several advantages for EV delivery compared to other commonly used hydrogel systems such as those based on polyethylene glycol (PEG), alginate, or collagen. HA-based hydrogels can support cell proliferation and differentiation (Uppal et al., 2011), whereas PEG-based hydrogels, though highly tunable and inert, lack inherent cell-interactive cues unless specifically functionalised (Stocke et al., 2017). Alginate and collagen hydrogels provide natural bioactivity but often exhibit less controllable mechanical properties and degradation profiles, which may limit sustained EV release(Kharkar et al., 2013). Tyramine modified HA enables enzymatic crosslinking via horseradish peroxidase (HRP) and hydrogen peroxide (H_2O_2), allowing for mild *in situ* gelation conditions that preserve EV integrity. *In situ* hydrogel formation in the presence of EVs helps to ensure EV encapsulation and the gelation can be conducted without covalent bonding to the encapsulated EVs. HA-TA hydrogels with low crosslinking density can also exhibit shear-thinning behavior with the potential to enable minimally invasive EV administration by injection (Kobayashi et al., 2020). Shear thinning allows a gel to flow under mechanical stress (e.g., during injection by syringe) and rapidly recover its structure once in place, making it particularly attractive for localised EV delivery.

Here, we examined HA-TA hydrogels as an EV delivery platform, aiming to achieve prolonged EV release and improved EV stability. HEK293T cells were selected as the source of EVs due to their rapid proliferation, high EV yield, and ease of genetic modification (Jurgielewicz et al., 2020). To quantify EVs, we obtained eGFP and luciferase-loaded EVs from lentivirus-transduced HEK293T cells, which were detectable using a luciferase assay. Hydrogel cytotoxicity was evaluated using ARPE-19 and H9c2 cell lines, given the potential applicability of this platform in ocular and cardiac applications. EVs were isolated through differential ultracentrifugation and characterised based on particle concentration, size, protein markers, and morphology. EVs were then encapsulated into HA hydrogels through pre- (*in situ*) and post-loading methods, and their stability was compared based on particle concentration, protein content, and cellular internalisation. Finally, EV-loaded HA hydrogels were assessed for their *in vitro* release profiles.

2. Materials and methods

2.1. Materials

HA (molecular weight of 200–400 kDa) was purchased from Glentham Life Sciences. Tyramine, 4-(4,6-dimethoxy-1,3,5-triazin-2-yl)-4-methylmorpholinium chloride (DMTMM), phosphate buffered saline (PBS), horseradish peroxidase (HRP; ≥250 units/mg solid), H_2O_2 (30 % w/v), deuterium oxide (D_2O), and sodium chloride were purchased from Sigma-Aldrich. 2-morpholinoethane sulfonic acid (MES) 1.0 M buffer solution (pH 5.5) was obtained from Alfa Aesar. Dulbecco's Modified Eagle Medium: Nutrient Mixture F-12 (DMEM/F12), Dulbecco's Modified Eagle's medium (DMEM), DMEM GlutaMax™ complete medium, Opti-MEM™, Dulbecco's phosphate-buffered saline (DPBS), fetal bovine serum (FBS), penicillin/streptomycin, PrestoBlue assay kits, MicroBCA protein assay kits, RIPA lysis buffer, poly-D-lysine (PDL) solution, and Hoechst dye were purchased from Thermo Fisher Scientific. Anti-CD9, anti-TSG101, and anti-calnexin antibodies were purchased from Abcam. Amicon Ultra 10 kDa centrifugal filters were obtained from Millipore. A 12–230 kDa Separation Module for simple WES was purchased from Bio-Techne. Luciferase assay was obtained from Promega. 4-chlorobenzenesulfonate salt (DiD) was obtained from Biotium. An ExoELISA complete kit (CD9 detection) was purchased from System Biosciences.

2.2. Synthesis and characterisation of HA-TA conjugates

Tyramine-modified HA was prepared following the protocol described by Ma et al. (2025). Hyaluronic acid sodium salt (50 mg, 0.124 mmol carboxyl groups) was dissolved in 5 mL MES buffer (100 mM, pH 5.5), followed by adding DMTMM (68.7 mg, 4 equivalents) for 10 min to activate the carboxylic acid groups. Tyramine solution (17 mg, 1 equivalent, 0.1 % w/v in MES buffer) was then added dropwise. After reacting for 24 h, the solution was enriched with 8 % v/v saturated sodium chloride and precipitated by adding three volumes of pure ethanol. The crude product was filtered through a Buchner funnel and sequentially washed with ethanol/water mixtures of 80/20 %, 96/4 %, and pure ethanol. The final precipitate was dried under vacuum for 24 h, yielding HA-TA as a white powder. This was stored at −20 °C. To determine the molar degree of substitution (DoS, %), HA-TA was dissolved in deuterium oxide (D_2O) at 0.4 % w/v, and was analysed by ^1H NMR spectroscopy (Bruker Avance Neo Nanobay 400). The N-acetyl proton on the glucosamine residue of HA was used as the internal standard, and the spectra were processed with MestReNova software. DoS was calculated by comparing the ratio of the integrated areas under the aromatic proton peaks at 6.90/6.88 ppm to N-acetyl proton peaks of HA at 2.0 ppm.

2.3. Synthesis and characterisation of HA-TA hydrogels

2.3.1. Hydrogel preparation

HA-TA hydrogels were prepared in PBS with 2 U/mL HRP at HA-TA concentrations of 0.25, 0.5, and 1 % w/v. Gelation was initiated by adding 0.05 mM H_2O_2 (in PBS) followed by a brief period of vortexing. The above gelation protocol was optimised and 0.05 mM H_2O_2 was found to be the minimum concentration required to achieve complete gelation, and thus was used in all experiments.

2.3.2. Morphology

100 μL of HA-TA hydrogels were prepared at concentrations of 0.25, 0.5, and 1 % w/v and immersed in 2 mL PBS at 37 °C for 48 h to reach swelling equilibrium. After that, the swollen gel was cut into thin slices with a thickness of 0.5 cm. The slices were then plunge-frozen in liquid nitrogen, and subsequently lyophilised for 72 h. Freeze-dried samples were mounted onto aluminium stubs with carbon-coated double-sided tape (TAAB). Samples were then coated with a Q150T 20 nm gold

sputter (Quorum) under an argon atmosphere. A FEI Quanta 200F field emission scanning electron microscope (SEM) connected to a secondary electron detector (Everheart-ThomLey Detector) was used to generate images of the materials. Images were taken at 200× magnification. Calculation of hydrogel mesh size was performed using the ImageJ software (National Institutes of Health) with a minimum sample size of 50.

2.4. Cell culture

Adult retinal pigment epithelial-19 (ARPE-19) cells were cultured in DMEM/F12 with 10 % v/v FBS and 1 % v/v penicillin/streptomycin. H9c2 cells were maintained in DMEM with 10 % v/v FBS and 1 % v/v penicillin/streptomycin, and human embryonic kidney (HEK293T) cells were grown in DMEM GlutaMax™ with 10 % v/v FBS and 1 % v/v penicillin/streptomycin. Cells were maintained in a 5 % CO_2 atmosphere at 37 °C and passaged upon reaching 80 % confluency.

2.5. In vitro cytotoxicity of HA-TA hydrogels

2.5.1. Preparation of leachable extracts of the hydrogel

Leachable extracts of hydrogel samples were prepared following ISO standards (British Standard, 2018). 1 mL hydrogel samples with concentrations of 0.25, 0.5, and 1 % w/v were immersed in 5 mL media at 37 °C for 48 h. Afterwards, the swollen hydrogels were carefully taken out, and the volume of media left was determined. Then, the volume of media that each 1 cm^2 hydrogel absorbs was calculated. Next, the volume of media the hydrogel absorbed was added to ensure a sufficient leaching volume. Hydrogel samples were immersed in complete DMEM media with surface to fluid volume ratio of 6 cm^2/mL. Samples were incubated at 37 °C for 72 h.

2.5.2. Cytotoxicity study

ARPE-19 or H9c2 cells (100 µL, 10,000 cells/well) were seeded into 96-well plates and incubated for 24 h. Afterwards, 100 %, 75 %, 50 %, 25 % v/v concentrations of liquid extracts were prepared by diluting with the complete media. 100 µL of these liquid extract samples were then added to each well of the plate and incubated for another 24 h before measuring the cell viability with the PrestoBlue assay.

2.6. Lentivirus-based gene transduction

2.6.1. Lentivirus production

For vector production, fifteen 100 mm dishes were seeded with 10^7 HEK293T cells in complete DMEM GlutaMax™ and left overnight to reach 70–80 % confluence. The cells were then triple transfected with 40 µg of the transfer vector plasmid carrying a transgene encoding a 2A bicistronic eGFP and luciferase genes and driven by the ubiqutous spleen focus forming virus promoter, 10 µg of the envelope plasmid PMD.G2, and 30 µg of the packaging construct plasmid p8.74 per dish. A transfection solution was prepared by adding 8 µL of a 10 mM polyethylenimine (PEI) stock to 40 mL of Opti-MEM™ and filtered through a 0.22 µm filter. This solution was then combined with the plasmid mixture and left at room temperature for 20 mins to make the transfection master mix. The cells were washed with DPBS, followed by the addition of Opti-MEM™ and 2.5 mL of transfection mix per dish for incubation. After 24 h, the transfection medium was replaced with fresh DMEM GlutaMax™. The viral-containing supernatant was collected 48 h post transfection, replenished with DMEM GlutaMax™, and supernatant was collected again after 24 h. The supernatant was then centrifuged at 3,000*g* for 10 min at room temperature and filtered through a 0.22 µm filter to remove cell debris. Finally, the collected supernatant was centrifuged at 3,000*g* and 4 °C for 18 h to pellet virus. The resulting pellet was resuspended in Opti-MEM™ and stored at −80 °C. The lentiviral titre was quantified using a viral p24 protein assay. The Zepto-Metrix p24 antigen enzyme linked immunosorbent assay (ThermoFisher Scientific) was used as per the manufacturer's protocol.

2.6.2. HEK293T cell transduction

HEK293T cells were seeded in a 6-well plate with 150,000 cells in 3 mL of complete DMEM GlutaMax™ per well. After incubating for 24 h, the cells were counted and the medium was refreshed. Lentiviral particles with multiplicity of infection (MOI) of 100 were added to three wells, with the remaining three serving as controls. After adding the viral particles, the plates were gently swirled and put in the incubator. The expression of lentiviral mediated enhanced green fluorescent protein (eGFP) was evaluated using a EVOS fluorescence microscope (Life Technologies) equipped with a filter set for eGFP detection (excitation maximum at 488 nm and emission maximum at 507 nm). Cells that were successfully transduced were then cultured in larger flasks for further experiments and EV production, while the non-transduced cells were cultured in parallel as controls.

2.7. Isolation and characterisation of EVs

2.7.1. Preparation of EV-depleted media

To deplete EVs in FBS, 20 % v/v FBS DMEM GlutaMax™ with 1 % v/v penicillin/streptomycin was ultracentrifuged at 100,000*g* and 4 °C for 18 h. Then, the supernatant was collected and filtered through 0.22 µm syringe filters. An equal volume of media (without FBS, with 1 % v/v penicillin/streptomycin) was added to the filtered media to prepare EV-depleted media containing 10 % v/v EV-depleted FBS, which was then stored at 4 °C and used within 4 weeks.

2.7.2. Isolation of EVs

EVs were produced from transduced HEK293T cells. Cells were cultured in EV-depleted media until reaching 80 % confluency. The cell culture supernatant was first spun at 300 g for 10 min to remove dead cells and cell debris. Post-spinning, the resulting supernatants were centrifuged at 2,000*g* for 10 min to further remove cell debris and apoptotic bodies. Subsequently, the supernatants were subjected to centrifugation at 16,500*g* for 30 min at 4 °C using the T-647.5 rotor on a Sorvall WX + Ultracentrifuge (Thermo Fisher Scientific) to remove large EVs. EVs were finally pelleted by ultracentrifugation at 100,000*g* for 155 min at 4 °C. The tubes were washed 2–3 times with 0.22 µm filtered DPBS, carefully avoiding the pellets. Then the pellets were resuspended in DPBS by repeated pipetting up and down and stored at −80 °C.

2.7.3. Nanoparticle tracking analysis (NTA)

NTA was performed using a NanoSight LM10 instrument (Malvern Panalytical) equipped with a sCOMs camera and a 532 nm green laser. 0.22 µm-filtered DPBS served as a negative control to examine the presence of particles (no more than 3 particles per frame of view). 1 mL of EV sample diluted in filtered DPBS was then analysed at a concentration ranging between 10^8 and 10^9 particles/mL (30–80 particles per frame of view), as recommended by the manufacturer. Optimal video capture settings (camera level between 14 and 16) and analysis parameters (detection threshold set at 4) were established for EV measurement. A 60-second video was recorded for each sample. This process was repeated to obtain a total of 6 videos per sample. The chamber was thoroughly cleaned between samples, first with MilliQ water and then with 20 % v/v ethanol/water, to prevent cross-contamination.

2.7.4. Transmission electron microscopy (TEM)

EVs resuspended in PBS were first fixed with 4 % v/v paraformaldehyde (PFA) solution. Then, one drop (25 µL) of the mixture was spotted onto parafilm. With forceps, a formvar carbon coated copper grid (400 mesh) was gently positioned on top of the drop for 2.5 min. The grid was positioned with the coated side facing the drop containing EVs. Two drops of water were placed on the parafilm and the grid was washed by sequentially positioning on top of the droplets for 30 s, and then moved onto 1 % v/v uranyl acetate (UA) for 2.5 min. Excess liquid

was removed using filter paper at 45°, and the grid was left to dry before analysis. Different magnifications were used for imaging, with micrographs recorded by Dr. Matt Hayes in the UCL Institute of Ophthalmology using a 100 kV JEOL-1010 TEM (JEOL).

2.7.5. Determination of EV proteins

EV samples were lysed by mixing with cold RIPA buffer in a 2:1 (v/v) ratio and incubating on ice for 15 min. Total protein concentration was determined using the MicroBCA protein assay kit according to the provided instructions. EV marker analysis was performed using the Simple Western system from Protein Simple (Biotechne Ltd), with a 12–230 kDa separation module and a 13-capillary cartridge, following the manufacturer's protocols. Primary antibodies were used to detect target proteins, including anti-CD9 (1:10 dilution), anti-TSG101 (1:50 dilution), and anti-Calnexin (1:100 dilution).

2.8. Preparation of EV-loaded hydrogels

To prepare EV-loaded hydrogels, 10^{11} particles/mL of EVs were embedded in 200 μL of HA-TA hydrogel with concentrations of 0.25, 0.5, and 1 % w/v. Two procedures were applied for embedding EVs in the gels. For pre-loaded hydrogels, HA-TA conjugates were mixed with EV particles in 200 μL of PBS with 2 U/mL HRP. Then, 0.05 mM H_2O_2 was added to initial the gel formation. For post-loaded hydrogels, the same hydrogel compositions were prepared without EVs, lyophilised, and then 200 μL of EV suspension in PBS was added to rehydrate the hydrogel.

2.9. Evaluation of EV stability after incorporation in hydrogels

200 μL of EV-loaded HA-TA hydrogels prepared by pre- and post-loading methods were incubated at 37 °C for 0, 1, 2, 4, and 7 days. Hydrogels were then degraded by adding 800 μL of 200 U/mL hyaluronidase, and the mixtures were placed on a shaker at 300 rpm overnight to ensure full degradation. After hydrogel degradation, EVs were concentrated by Amicon Ultra 10 kDa centrifugal filters following the manufacturer's instructions. Hydrogels without EVs were degraded in parallel and served as the control. Fresh EV samples with the same concentration were placed at 37 °C for 7 days for comparison. The stability of the EV components was assessed by NTA and WES as detailed in Sections 2.7.3 and 2.7.5.

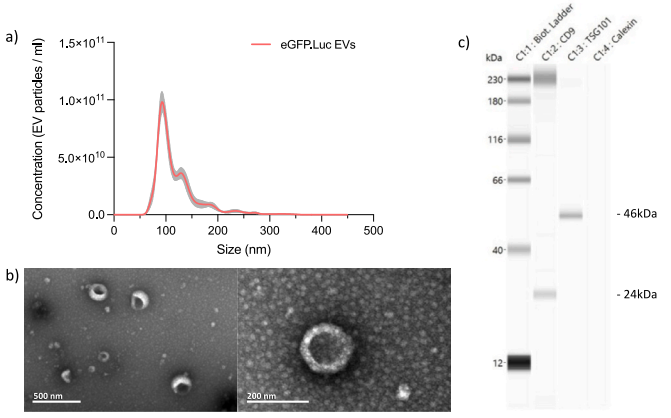

Fig. 1. (a) Particle size distribution of EVs. The grey area denotes the SD values. Raw data were collected from Nanosight and processed by Prism. (b) Representative TEM images of EVs isolated from transduced HEK293T cells with scale bars of 500 nm (left) and 200 nm (right). (c) Simple Western blotting of EV-specific markers CD9 and TSG101, which are indicative of EVs, and calnexin, a marker for endoplasmic reticulum vesicles. The detection of CD9 and TSG101 confirms the vesicular nature of the samples, while the absence of calnexin suggests that there is no endoplasmic reticulum vesicle contamination in the EV preparations.

2.10. In vitro internalisation of EVs

2.10.1. Luciferase assay system

Internalisation of EVs was analysed by quantifying the amount of functional luciferase using the luciferase assay system. The internalisation was measured by incubating different doses of EVs with cells for 1 h. The uptake dynamic was measured by incubating EVs (10^{10} particles/mL) with cells for various time points (0.25, 1, 2, 6, 12 and 24 h). ARPE-19 and H9c2 cells were seeded at 10,000 cells in 100 μL of complete media / well in a white 96-well plate for 24 h. Following incubation, the media was removed, and the cells were washed twice with DPBS. Subsequently, 100 μL of EVs in EV-depleted media was added to each well and incubated. After this incubation, the supernatant was removed, the wells were washed twice with DPBS, and the supernatant was retained for subsequent analysis. Cells were then lysed by adding 20 μL lysis buffer to each well for 15 min on ice. Additionally, 10 μL of the supernatant was also lysed using 10 μL of lysis buffer to quantify any uninternalised EVs. Finally, 100 μL of luciferase assay reagent was added to each sample, mixed well and the luminescence was measured using a GloMax 20/20 luminometer (Promega). Luminescence from cells incubated with naive EVs served as a negative control.

2.10.2. In vitro internalisation of hydrogel released EVs

To evaluate the uptake of EVs released from hydrogels, 200 μL of EV-loaded HA-TA hydrogels (0.25 % w/v) were added to the wells of a 48-well plate. Each hydrogel sample contained 10^{11} particles/mL of EVs. 300 μL of PBS was added to each well, and the plate incubated in a chamber at 37 °C, with a shaking speed of 150 rpm. After 24 h, the supernatant was collected and concentrated using Amicon 10 kDa filters. The concentration of collected EVs was quantified by NTA. For internalisation studies, both ARPE-19 and H9c2 cells (10,000 cells per well) were exposed to the released EVs at a concentration of 10^{11} particles/mL (100 μL) for 1 h. The uptake was then measured by the luciferase assay as detailed in Section 2.10.1.

2.10.3. Hydrogel released EVs visualised by confocal microscopy

Hydrogel released EVs were stained using DiD. For the staining process, EV pellets were resuspended in 1 mL of PBS with DiD dye at a concentration of 5 μg/mL and incubated for 10 min. Subsequently, DiD-labeled EVs were pelleted by ultracentrifugation at 100,000 g for 70 min at 4 °C. To remove excess dye, the pellet was then washed in 0.22 μm filtered PBS and subjected to centrifugation at 150,000*g* for 90 min at 4 °C.

ARPE-19 or H9c2 cells (100,000 cells/well in 4 mL media) were seeded on PDL-coated cover glasses placed in 6-well plates and cultured for 24 h prior to starting the experiment. Next, cells were treated with DiD-labelled EVs for 1 h. Afterwards, the medium was discarded and the cells were washed with DPBS three times to remove any uninternalised EVs. Subsequently, the cells were incubated with fresh medium containing Hoechst dye (4 drops/2 mL of medium) for 20 min to stain the cell nuclei. Cellular uptake was observed using a confocal microscope (Zeiss LSM 710), with a Plan-Apochromat objective 63×/1.4 Oil DICII.

2.11. Release of EVs from HA-TA hydrogel

EV suspensions at 10^{11} particles/mL were loaded in 200 μL of HA-TA hydrogels with concentrations of 0.25, 0.5, and 1 % w/v, and then crosslinked in a 48-well plate. Then, 300 μL of PBS was added to each well, and the plate was incubated in a chamber at 37 °C with a shaking speed at 150 rpm. At different time points (1, 3, 6, 12 h and 1, 2, 4, 7 days), the entire volume of PBS was collected and replaced with fresh pre-heated PBS. Quantification of released EVs was performed using an ExoELISA complete kit (CD9 detection). Instead of using the provided protein standards, isolated EVs were used and prepared at

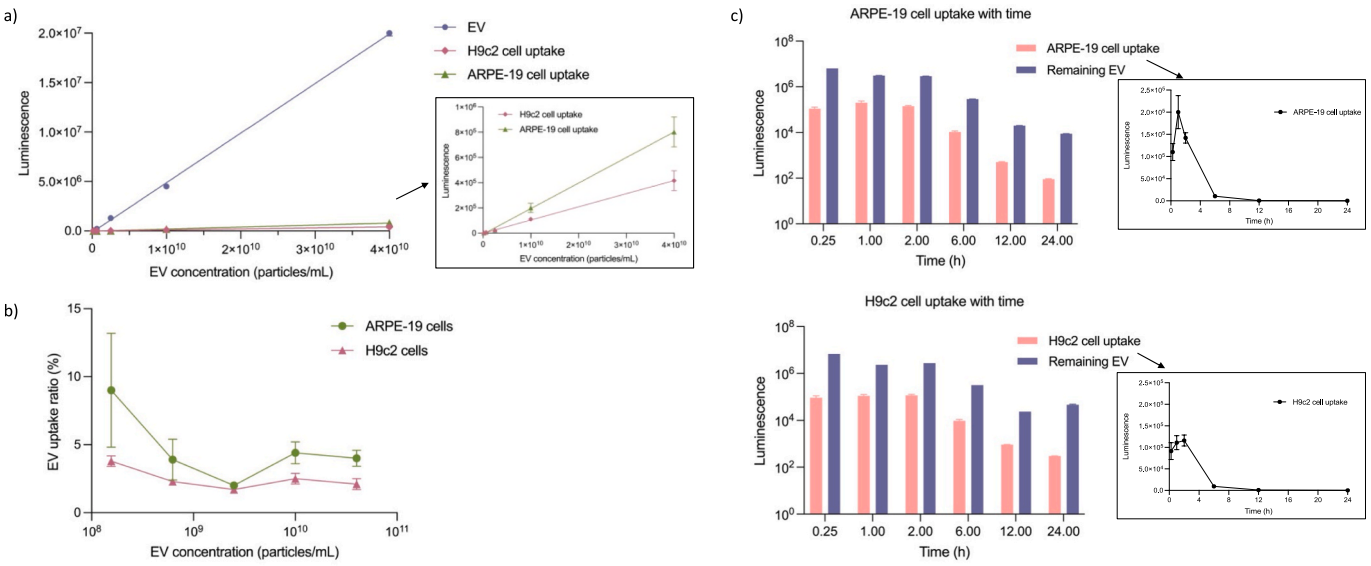

Fig. 2. (a) Dose-response uptake study. Different doses of EVs were incubated with ARPE-19 or H9c2 cells for 1 h. The correlation of EV concentration to luminescence was determined by the luciferase assay. (b) The percentage of EV uptake by ARPE-19 cells and H9c2 cells. (c) A kinetic study of EV uptake by APRE-19 and H9c2 cells. ARPE-19 and H9c2 cells were incubated with EVs (10^{10} particles/mL) at 37 °C to monitor EV internalisation, quantified using a luciferase assay. The pink bars represent the uptake of EVs by cells, while the purple bars indicate the remaining EVs in the supernatant. The y-axis of the bar graphs is on a logarithmic scale, and the inset line chart depicts the uptake dynamics to illustrate the progressive internalisation of EVs by the cells. Data are presented as mean ± SD, with experiments conducted using three independent plates, each containing two wells per plate (n = 6). Some of the error bars are too small to be seen. (For interpretation of the references to colour in this figure legend, the reader is referred to the web version of this article.)

concentrations of 5.42×10^{10}, 3.61×10^{10}, 2.71×10^{10}, 1.81×10^{10}, 9.03×10^{9}, 4.51×10^{9}, 2.26×10^{9}, and 0 particles/mL following the manufacturer's instruction.

2.12. Statistical analysis

All statistical analyses were performed using GraphPad Prism software (version 10.4.0.527). For multiple group comparisons, one-way ANOVA followed by Tukey's post hoc test was applied. A significance level of $p < 0.05$ was used; differences not meeting this threshold were reported as "not significant (n.s.)".

3. Results and discussion

3.1. Characterisation of EVs

Successful HEK293T cell transduction was initially confirmed by visualising the eGFP protein using fluorescence microscopy (Supporting Information, Fig. S1). According to the guidelines published by the International Society for Extracellular Vesicles in 2018 (MISEV2018), several quality control parameters are required for the identification of EVs, including quantification of protein content and particle number, purity determination, protein marker evaluation, and characterisation of single vesicles (Théry et al., 2018).

NTA results of EVs isolated from the transduced cells (Fig. 1a) indicate that the majority of the isolated particles were distributed within the size range reported in the literature for EVs (40–150 nm) (Pegtel and Gould, 2019). The mean and mode sizes of the EVs were 119.0 nm and 92.9 nm respectively. The protein content of the EVs was quantified by MicroBCA assay. These protein concentration values were then used to calculate and evaluate the purity of the samples, expressed as the particle-to-protein ratio. The obtained EV particle-to-protein ratio was 4.1×10^{9} particles/μg of protein (calculations are shown in Table S1). Work by Webber and Clayton (2013) stated that ratios below 1.5×10^{9} particles/μg of protein are indicative of impure samples. These results demonstrate that the isolated particles meet the criteria for purity, and that the isolation method effectively removed the majority of contaminated proteins from the sample.

TEM is regarded as the benchmark for single EV visualisation and was used in this study to assess EV size, morphology, and sample purity. Fig. 1b reveals a characteristic cup-shaped appearance of the EVs. The size distribution histogram (Fig. S2) from TEM reveals most vesicles are within the 40–150 nm range, which is consistent with NTA data and sizes reported in literature (Li et al., 2016). Fig. 1c shows a representative western blot of EVs isolated from transduced HEK293T cells. The presence of the transmembrane protein CD9 is consistent with the lipid bilayer constitution of the EVs, and the presence of cytosolic TSG101 confirms that these lipid bilayers encased intracellular components (Théry et al., 2018). The absence of a protein band around the molecular weight of approximately 90 kDa confirms that calnexin was not present in the EV preparations. This further proves that the isolated particles were indeed EVs rather than vesicle contaminations from other cellular compartments (Lässer et al., 2012).

3.2. In vitro internalisation of EVs

To confirm the capability of EVs to be internalised by different cell types, *in vitro* cell uptake of EVs was explored in terms of both dose–response and kinetic experiments. Cellular internalisation of EVs is important as it enables their interaction with target cells and promoting biological responses. Specifically, in this study, understanding EV internalisation is crucial for evaluating their release from the HA-TA hydrogel and subsequent bioactivity, as effective cellular uptake is essential for the therapeutic efficacy of EV-loaded hydrogels. ARPE-19 cells and H9c2 cells are useful in ocular and cardiovascular research where EV-based therapies might be utilised. These cell lines were used as *in vitro* models to explore the versatility and efficacy of HEK293T-derived EVs. The calibration curve of luminescence vs EV concentration (purple line, Fig. 2a) confirmed the presence of luciferase in the EVs. Thus, the luciferase enzyme can be measured and quantified upon EV lysis by the luciferase assay. The luminescence of the cells increased proportionally with the EV concentrations, indicating successful internalisation of the EVs by both ARPE-19 and H9c2 cells. Saturation was not observed even at the highest EV concentrations (4×10^{10} particles/

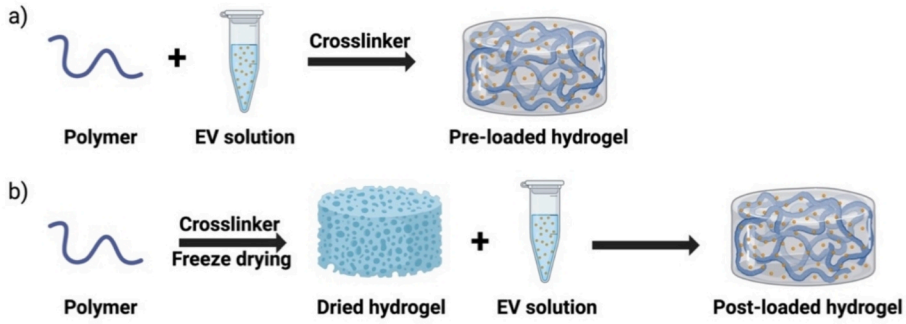

Fig. 3. Schematic illustration of pre-loaded and post-loaded hydrogels for encapsulating EVs. (a) Pre-loading hydrogels were formed by mixing EVs directly with HA-TA conjugates and HRP, and then adding the crosslinking reagent H_2O_2. (b) Post-loading hydrogels were formed by adding EV suspensions to lyophilised hydrogels.

mL).

The inset panel on the right of Fig. 2a provides an enlarged view of the cell uptake data. The EV uptake by ARPE-19 (green line) and H9c2 cells (pink line) shows that the EV uptake by both cell lines increased proportionally with the dose of EVs. Moreover, ARPE-19 cells exhibited a higher uptake capacity for EVs, approximately double that of H9c2 cells. Fig. 2b shows the internalisation ratios of both cell types compared with the EV calibration curve at different doses. There is no consistent trend. The uptake of EVs by ARPE-19 cells at the highest concentration (4×10^{10} particles/mL) was 4.0 % ± 0.6 %, while it is lower for H9c2 cells at 2.1 % ± 0.4 %. Notably, at the lowest concentration (1.6×10^{8} particles/mL), ARPE-19 cells show an increase in uptake to 9.0 % ± 4.2 %, and H9c2 cells to 3.8 % ± 0.4 %, suggesting a non-linear uptake pattern across EV concentrations. However, it should also be noted that the total percentage of remaining EVs in the supernatant plus the internalised EVs was substantially less than 100 %, which could be attributed to losses during the DPBS washing steps (Table S2). The washing step was intended to remove unbound or loosely attached EVs, but can also remove bound EVs that have not yet been internalised. Additionally, EV internalisation is a dynamic process with continuous binding, uptake, and possibly recycling of vesicles to and from the cell surface, which could also contribute to the percentages being lower than might be expected.

The kinetics of the EV uptake process are depicted in Fig. 2c. The pink bars demonstrate immediate EV internalisation from as early as 15 min after initial introduction, which correlates with evidence from other studies (Fabbri et al., 2012; Feng et al., 2010). This is seen with both ARPE-19 and H9c2 cells. The internalisation reached a peak at 1 h for ARPE-19 cells and at 2 h for H9c2 cells, and then decreased thereafter. The process was completed by 24 h, when all EVs were internalised and almost no EVs remained in the supernatant at this point (Fig. 2c, right panels). The purple bars indicate a rapid drop in luminescence from EVs in the media, particularly from 0.25 h to 1 h for ARPE-19 cells and up to 2 h for H9c2 cells. This suggests rapid initial internalisation of EVs into both cells, resulting in a decrease in the number of EVs in the supernatant. The EV amounts in the supernatant have markedly decreased at 12 h, suggesting that the majority of EV internalisation occurs in the initial 12 h. The correlation is further supported by the inset graphs, which shows that almost all EVs were internalised by cells in 12 h, aligning with the lower levels of remaining EVs in the supernatant at this time point.

3.3. Preparation of EV-loaded hydrogels

EVs were encapsulated into the hydrogels using both pre- and post-loading methods, as illustrated in Fig. 3. In the pre-loading method (Fig. 3a), EVs were mixed directly with the hydrogel precursor solution (HA-TA conjugate), followed by crosslinking with HRP and H_2O_2. This method can also be adapted for *in situ* formation using a double-chamber syringe, where the EVs and polymer solution are in one chamber and the crosslinker solution is in another, allowing for simultaneous injection. The post-loading method (Fig. 3b), also known as the "breathing method", used lyophilised hydrogels, which are rendered porous through water removal. The EV solution is directly added to the dried hydrogel, allowing the EVs to be absorbed into the hydrogel matrix.

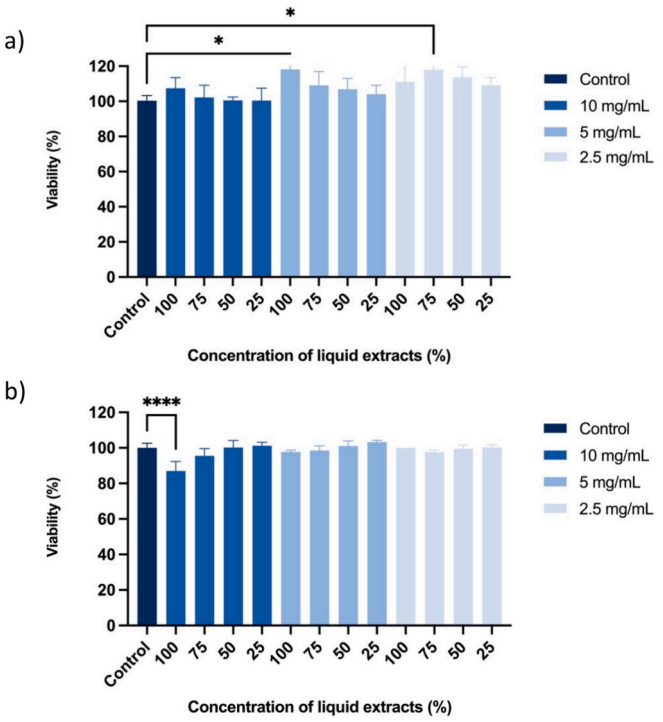

Fig. 4. Liquid extracts prepared from HA-TA hydrogels with concentrations of 2.5, 5, and 10 mg/mL were incubated with (a) ARPE-19 cells and (b) H9c2 cells for 24 h. Data are presented as mean ± SD (n = 3). Statistical analysis was performed using one-way ANOVA and Tukey's multiple comparisons test, *$p \leq 0.05$, ****$p \leq 0.0001$.

3.4. Hydrogel cytotoxicity

The hydrogel solution was composed of HA-TA, HRP and the initiator H_2O_2. HA, TA and HRP have been shown to be biocompatible and non-immunogenic (Darr and Calabro, 2009), but the initiator H_2O_2 is potentially cytotoxic (Gardner et al., 1997). Therefore, it is important to evaluate the cytotoxicity of leachable components of the hydrogel.

In general, Fig. 4 displays no significant difference in cell viability across all concentrations of hydrogel extracts compared to the control, indicating that the extracts are well tolerated by both cell lines. However, a statistically significant increase in ARPE-19 viability is observed

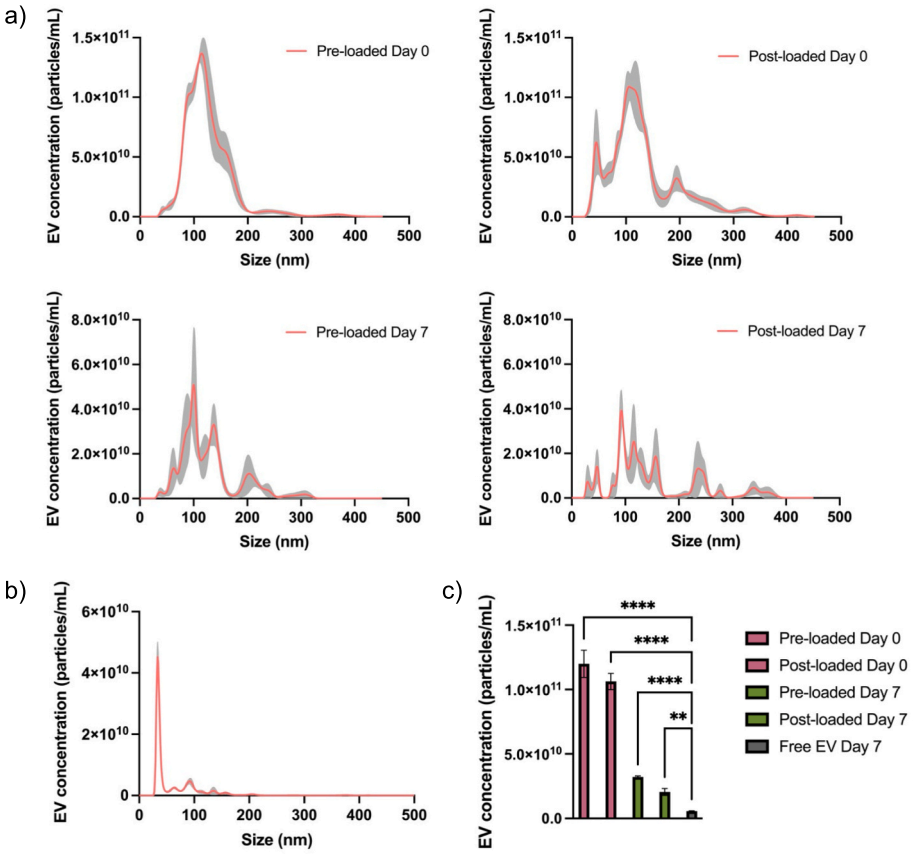

Fig. 5. (a) NTA data of hydrogel encapsulated EVs at day 0 and day 7, (b) free EVs on day 7, and (c) the concentrations of EVs recovered from the gels and free EVs. Hydrogels were composed of 10 mg/mL HA-TA and were incubated at 37 °C. Data are presented as mean ± SD (n = 5). **p ≤ 0.01, ****p ≤ 0.0001.

between the control and the 100 % extract concentrations for the 5 mg/mL hydrogel and 75 % extract concentrations for the 2.5 mg/mL hydrogel, suggesting that hydrogel extracts may promote proliferation in ARPE-19 cells. In contrast, H9c2 cells treated with the 100 % extract concentrations from the 10 mg/mL hydrogel show a significant viability decrease, which may be attributed to the diluted media used in producing hydrogel extracts. Overall however, the hydrogels are generally nontoxic to both ARPE-19 and H9c2 cells and exhibit good cytocompatibility.

3.5. Evaluation of EV stability after incorporation in hydrogels

3.5.1. NTA of EVs loaded in hydrogels over time

EV-loaded hydrogels made from 10 mg/mL HA-TA were first formulated using both the pre- and post-loading methods, and then subjected to degradation using hyaluronidase on either day 0 or day 7. After concentration using Amicon centrifuge filters, NTA (Fig. 5) was employed to evaluate the size distribution and particle concentration of EVs encapsulated within the hydrogels, comparing the initial measurements on day 0 with those on day 7 to analyse any changes in particle size and concentration over time.

Fig. 5a and b display the size distribution of encapsulated EVs and free EVs, while Fig. 5c presents the particle concentrations. On day 0, pre-loaded EVs exhibit a monodisperse size distribution, indicating uniform vesicle size and stability during the pre-loading process. The particle concentration remained unchanged at 1.2×10^{11} particles/mL, closely matching the initial loading concentration of 1.0×10^{11} particles/mL. The post-loaded EVs maintained a similar particle concentration at 1.0×10^{11} particles/mL while displaying a broader size distribution, suggesting potential EV aggregation, with both smaller (~50 nm) and larger (~200 nm) fractions. By day 7, the size distribution of EVs in both pre-loaded and post-loaded hydrogels had broadened, indicating increased size heterogeneity and evidence of particle degradation and aggregation over time. Notably, particle concentrations decreased to 3.2×10^{10} particles/mL in the pre-loaded gel and 2.0×10^{10} particles/mL in the post-loaded gel.

The crosslinked network of a hydrogel can restrict the movement of EVs, aiding in their preservation by creating a spacing between EV particles, thereby preventing aggregation. Without encapsulation, EVs suspended in PBS tend to aggregate with consequent membrane rupture (Wu et al., 2021). The HA-TA hydrogel has a pore size of around 200 μm (Fig. S3), which is unable to limit EV movement as effectively as hydrogels with smaller pores. However, our hydrogels still preserve EVs, with higher concentrations observed compared to free EVs, where a significant decrease in EV concentration from 1.0×10^{11} particles/mL to 5.7×10^{9} particles/mL was seen after 7 days of storage at 37 °C. A multimodal EV particle size distribution is expected after 7-days of storage in hydrogels at 37 °C. This is attributed to some EVs possibly undergoing fusion to form larger vesicles or fragmentation into smaller ones, while others possibly experienced degradation.

3.5.2. Protein content

EV are membrane structured vesicles encapsulating proteins, nucleic acids and lipids (Kalluri and LeBleu, 2020). In suspension, they undergo irregular Brownian motion, leading to aggregation and potential rupture of their membrane structure. This can inactivate their contents in the absence of protective mechanisms (Maroto et al., 2017). For instance, EVs stored in PBS at 37 °C often show significant activity loss within a few days. HA-TA hydrogels can enhance EV stability by offering multiple protective mechanisms. First, the hydrogel provides a hydrated environment that minimises desiccation and shields EVs from environmental stress. Second, the crosslinked polymer network limits the infiltration of

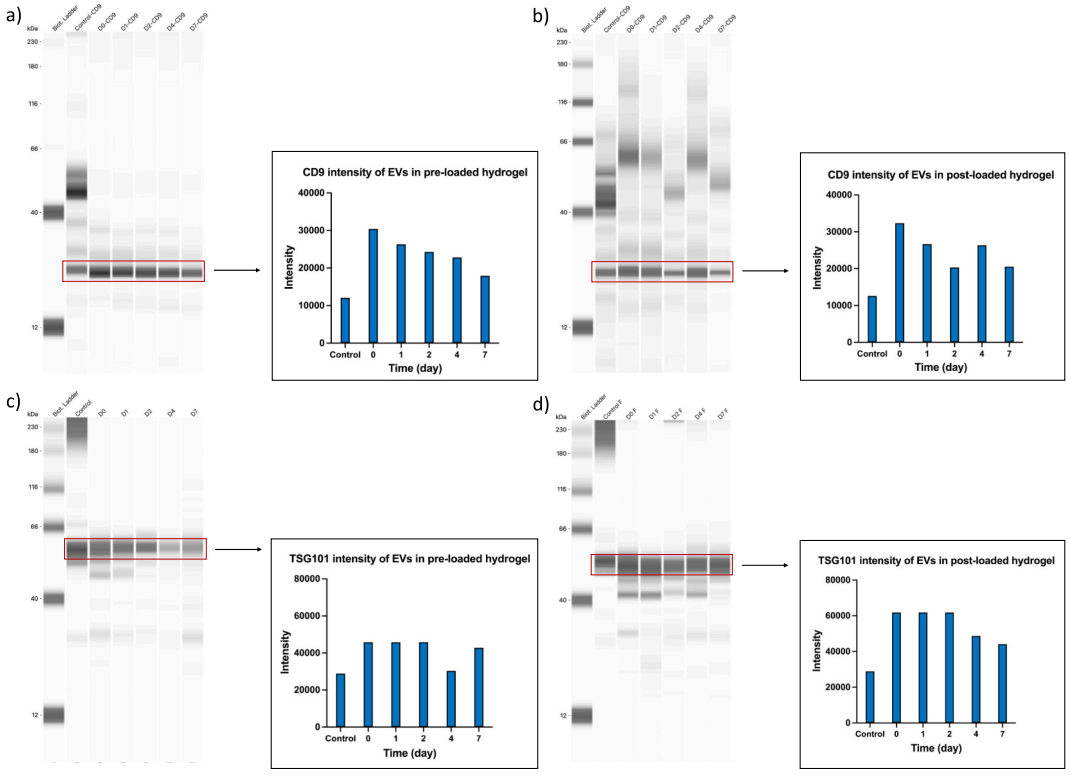

Fig. 6. Simple WES images of CD9 protein marker in EVs encapsulated in (a) pre-loaded and (b) post-loaded hydrogels, and TSG101 protein marker in EVs encapsulated in (c) pre-loaded and (d) post-loaded hydrogels. Hydrogels were composed of 10 mg/mL HA-TA and were incubated at 37 °C. Hydrogels without EVs degraded and concentrated using the same method served as the control. Bar graphs represent semi-quantitative densitometry analysis of representative western blots. **p ≤ 0.01, ****p ≤ 0.0001.

degradative agents such as enzymes and ions, helping to prevent premature degradation of EV contents (Su et al., 2010). Additionally, the restricted mobility of EVs within the hydrogel matrix reduces their likelihood of aggregation. These combined effects contribute to the improved preservation of EV structure, stability, and bioactivity over extended storage periods.

CD9 and TSG101 are protein markers commonly used to evaluate the presence and integrity of EVs (Sivanantham and Jin, 2022). CD9 is typically found on the membrane of EVs (Escola et al., 1998), and TSG101 is packaged inside (Katzmann et al., 2001). If EVs degrade over time, their protein levels, particularly TSG101, may decrease as the proteins are released into the surrounding environment. Furthermore, a decrease in CD9 levels would also suggest the loss of EV integrity or a reduction in EV numbers. EVs were encapsulated in 10 mg/mL HA-TA hydrogels by pre- and post-loading strategies, and were then digested on different days. After concentration using Amicon centrifuge filters, WES was utilised to evaluate the protein content of the EVs. This analysis compared the initial measurements on day 0 with those on day 1, 2,

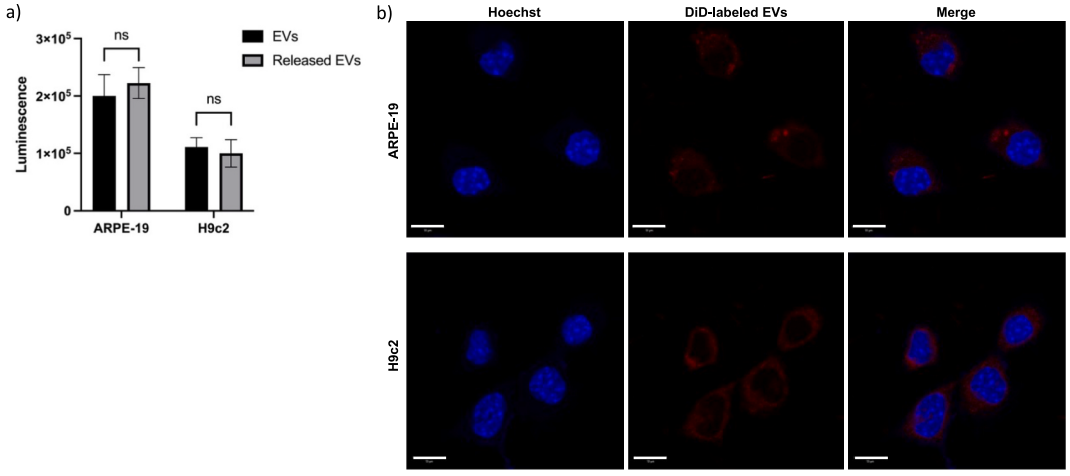

Fig. 7. (a) The internalisation of fresh EVs and EVs released from a pre-loaded 2.5 mg/mL w/v gel by ARPE-19 and H9c2 cells. Data are presented as mean ± SD, with experiments conducted using three independent plates, each containing two wells per plate (n = 6). (b) Representative confocal images showing the uptake of DiD-labeled EVs released from the hydrogel by ARPE-19 (top) and H9c2 (bottom) cell lines. Cells were incubated with DiD-labeled EVs (red) for 1 h. After incubation, the cells were washed, fixed and stained with Hoechst dye (blue) to mark the nuclei. Scale bar = 10 μm. (For interpretation of the references to colour in this figure legend, the reader is referred to the web version of this article.)

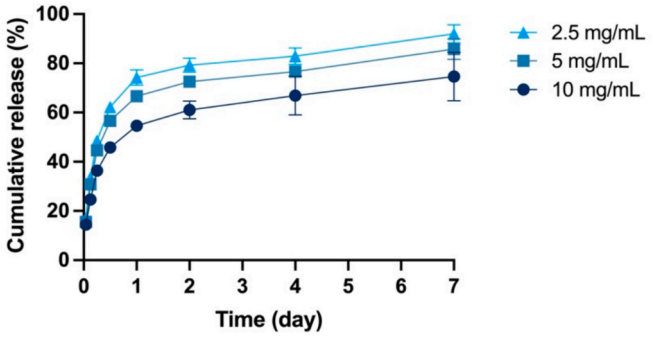

Fig. 8. *In vitro* cumulative release profile of EVs from pre-loaded HA-TA hydrogels with concentrations of 2.5, 5, and 10 mg/mL over 7 days. Data are presented as mean ± SD (n = 3).

4, and 7 to identify any changes over time.

As shown in Fig. 6a and b, the overall CD9 intensity generally decreased with time, though the trends are a little complex. For TSG101, as depicted in Fig. 6c and d, the intensity remained constant during the first two days. In the case of the post-loaded gels this is followed by a decrease in intensity, while for the pre-loaded gel the intensity remains more constant. The decline in protein intensity suggests some extent of degradation and reduced stability of the EVs within the hydrogel over time. However, free EVs (that were not encapsulated into the hydrogels) incubated for 7 days at 37 °C showed no detectable protein bands (Fig. S4). Therefore, compared with free EVs, embedding the EVs in the hydrogels can enhance their stability in terms of key protein levels, as well as the overall EV number (Fig. 6). The literature indicates that EVs embedded in a gelatin methacryloyl hydrogel demonstrated no significant change in protein expression compared to EVs in PBS at 4 °C (Wu et al., 2021). To our knowledge, our study is the first to elucidate the broad preservation of EV protein content in hydrogels at 37 °C over 7 days.

3.6. *In vitro internalisation of EVs released from hydrogel*

The data above show that both pre- and post-loading methods can preserve EV stability compared to free EVs. Since hydrogels prepared by pre-loading allow for *in situ* injection and there is potentially some advantage in terms of EV stability, it was decided to use these for the following EV internalisation and release studies. A pre-loaded gel prepared at 2.5 mg/mL was incubated for 24 h, and the released vesicles recovered and explored in cell uptake assays. The lower concentration of 2.5 mg/mL HA-TA was used for this study because it was expected to allow for faster release of EVs, enabling the collection of a larger quantity of EVs within the 24-hour incubation period. The *in vitro* uptake of hydrogel-released EVs was assessed by the luciferase assay and confocal microscopy. Fig. 7a demonstrates that both ARPE-19 and H9c2 cells can internalise the released EVs, with no significant difference in the uptake level compared with free EVs. These results indicate that incorporation of EVs into the hydrogel delivery system does not affect their cellular uptake, and suggests potential for therapeutic applications.

Hoechst dye was employed to stain the nucleus blue, and EVs released from the hydrogel were labelled with DiD to fluoresce red. After co-incubation for 1 h, Fig. 7b shows the confocal microscopy images obtained. There is a uniformity of red fluorescence in the perinuclear regions across the cells, suggesting uptake of released EVs. The specificity of the red fluorescence to the cells indicates successful labelling and the potential of EVs to be internalised by both cell types.

3.7. *Time-resolved in vitro EV release*

The protein contents of CD9 and CD63 were first measured by Simple WES to select the protein with the highest expression. CD63 expression was undetectable while CD9 was found to be highly expressed in the isolated EVs (Fig. S5). Therefore, CD9 was selected for quantification in this study (Fig. 8).

Fig. 8 illustrates that the release profile of EVs from hydrogels of varying polymer concentrations follows a similar trend, with a burst initial release within the first day followed by a deceleration over time. By modulating the polymer concentration of the system, the cumulative release of EVs can be varied. Specifically, hydrogels composed of 2.5 mg/mL HA-TA exhibited the most rapid release rate and 92.0 ± 3.6 % of the EVs were released over 7 days. Hydrogels with a higher polymer concentration of 10 mg/mL HA-TA demonstrated a slower release rate, with 74.6 ± 9.8 % of EVs released in the same period. The slower release from the hydrogels with higher HA-TA concentration may be attributed to the increased density of the hydrogel matrix (Fig. S3), which creates a more restrictive environment for EV diffusion This observation aligns with studies indicating that hydrogels composed of higher polymer concentrations (4 % w/v alginate), demonstrated a notably extended retention time of EVs compared with those formed with lower alginate concentrations (2 % w/v) (Huang et al., 2021). The trend suggests that hydrogel concentration plays a role in modulating the release of EVs, which is an important consideration for therapeutic applications where controlled release is desired.

4. Conclusion

In this study, we successfully isolated eGFP and luciferase-loaded EVs from stably transduced HEK293T cells and encapsulated them into HA-TA hydrogels via pre- and post-loading methods. The EVs retained their size distribution, and protein marker expression over 7 days when encapsulated in the hydrogel. We observed notably enhanced stability of gel-encapsulated EVs compared to free EVs in solution, which exhibited a tenfold decrease in particle concentration, increased heterogeneity, and undetectable protein intensity. Encapsulated EVs were effectively internalised by ARPE-19 and H9c2 cells, indicating preserved bioactivity after hydrogel loading and release. Internalisation levels were comparable to those of fresh EVs, as confirmed by luciferase assays and visualised using confocal microscopy. EV pre-loaded pre-loaded hydrogels, designed for potential *in situ* applications, demonstrated controlled release over a period of 7 days. Tunable release kinetics could be obtained through variation in the HA-TA concentration. The *in situ* gelation capability of pre-loaded HA-TA hydrogels makes this platform particularly attractive for localised delivery to delicate or hard-to-access tissues, such as ocular or myocardial sites. These findings support the use of HA-TA hydrogels as a versatile and minimally invasive strategy worthy of further study.

While this study demonstrates promising results *in vitro*, further investigations in *in vivo* models are needed to evaluate the biodistribution, immunogenicity, and long-term therapeutic efficacy of the encapsulated EVs. Additionally, standardisation of EV loading efficiency and hydrogel degradation profiles across different biological environments will be crucial for future translational applications.

CRediT authorship contribution statement

Yingchang Ma: Writing – review & editing, Writing – original draft, Visualization, Methodology, Investigation, Formal analysis, Conceptualization. **Ines Colic:** Writing – review & editing, Methodology, Investigation. **Maha Muwaffak:** Resources, Methodology, Investigation. **Ahad A. Rahim:** Writing – review & editing, Supervision, Resources, Project administration, Methodology, Conceptualization. **Steve Brocchini:** Writing – review & editing, Supervision, Resources, Project administration, Funding acquisition, Conceptualization. **Gareth R. Williams:** Writing – review & editing, Supervision, Resources, Project administration, Conceptualization.

Declaration of competing interest

The authors declare that they have no known competing financial interests or personal relationships that could have appeared to influence the work reported in this paper.

Acknowledgements

The authors thank the Engineering and Physical Sciences Research Council for the award of PhD studentships to IC and MM as part of the Centre for Doctoral Training in Advanced Therapeutics & Nanomedicines (EP/L01646X/1).

Appendix A. Supplementary material

Supplementary material to this article can be found online at https://doi.org/10.1016/j.ijpharm.2025.125650.

Data availability

Data will be made available on request.

References

British Standard, 2018. Biological evaluation of medical devices [WWW Document]. https://www.iso.org/obp/ui#iso:std:iso:10993:-1:ed-5:v2:en (accessed 6.13.24).
Chen, P., Wang, L., Fan, X., Ning, X., Yu, B., Ou, C., Chen, M., 2021. Targeted delivery of extracellular vesicles in heart injury. Theranostics 11, 2263. https://doi.org/10.7150/thno.51571.
Choi, K.Y., Han, H.S., Lee, E.S., Shin, J.M., Almquist, B.D., Lee, D.S., Park, J.H., 2019. Hyaluronic acid–based activatable nanomaterials for stimuli-responsive imaging and therapeutics: Beyond CD44-mediated drug delivery. Adv. Mater. 31, 1803549. https://doi.org/10.1002/adma.201803549.
Darr, A., Calabro, A., 2009. Synthesis and characterization of tyramine-based hyaluronan hydrogels. J Mater Sci: Mater Med 20, 33–44. https://doi.org/10.1007/s10856-008-3540-0.
Das, C.K., Jena, B.C., Banerjee, I., Das, S., Parekh, A., Bhutia, S.K., Mandal, M., 2019. Exosome as a novel shuttle for delivery of therapeutics across biological barriers. Mol. Pharm. 16, 24–40. https://doi.org/10.1021/acs.molpharmaceut.8b00901.
Deng, G., Li, F., Yu, H., Liu, F., Liu, C., Sun, W., Jiang, H., Chen, Y., 2012. Dynamic hydrogels with an environmental adaptive self-healing ability and dual responsive sol–gel transitions. ACS Macro Lett. 1, 275–279. https://doi.org/10.1021/mz200195n.
Escola, J.M., Kleijmeer, M.J., Stoorvogel, W., Griffith, J.M., Yoshie, O., Geuze, H.J., 1998. Selective enrichment of tetraspan proteins on the internal vesicles of multivesicular endosomes and on exosomes secreted by human B-lymphocytes. J. Biol. Chem. 273, 20121–20127. https://doi.org/10.1074/jbc.273.32.20121.
Fabbri, M., Paone, A., Calore, F., Galli, R., Gaudio, E., Santhanam, R., Lovat, F., Fadda, P., Mao, C., Nuovo, G.J., Zanesi, N., Crawford, M., Ozer, G.H., Wernicke, D., Alder, H., Caligiuri, M.A., Nana-Sinkam, P., Perrotti, D., Croce, C.M., 2012. MicroRNAs bind to Toll-like receptors to induce prometastatic inflammatory response. Proc. Natl. Acad. Sci. U.S.A. 109. https://doi.org/10.1073/pnas.1209414109.
Fakhari, A., Berkland, C., 2013. Applications and emerging trends of hyaluronic acid in tissue engineering, as a dermal filler and in osteoarthritis treatment. Acta Biomater. 9, 7081–7092. https://doi.org/10.1016/j.actbio.2013.03.005.
Feng, D., Zhao, W.L., Ye, Y.Y., Bai, X.C., Liu, R.Q., Chang, L.F., Zhou, Q., Sui, S.F., 2010. Cellular internalization of exosomes occurs through phagocytosis. Traffic 11, 675–687. https://doi.org/10.1111/j.1600-0854.2010.01041.x.
Gardner, A.M., Xu, F., Fady, C., Jacoby, F.J., Duffey, D.C., Tu, Y., Lichtenstein, A., 1997. Apoptotic vs. nonapoptotic cytotoxicity induced by hydrogen peroxide. Free Radical Biology and Medicine 22, 73–83. https://doi.org/10.1016/s0891-5849(96)00235-3.
Huang, C.C., Kang, M., Shirazi, S., Lu, Y., Cooper, L.F., Gajendrareddy, P., Ravindran, S., 2021. 3D Encapsulation and tethering of functionally engineered extracellular vesicles to hydrogels. Acta Biomater. 126, 199–210. https://doi.org/10.1016/j.actbio.2021.03.030.
Ju, Y., Hu, Y., Yang, P., Xie, X., Fang, B., 2023. Extracellular vesicle-loaded hydrogels for tissue repair and regeneration. Mater. Today Bio 18, 100522. https://doi.org/10.1016/j.mtbio.2022.100522.
Jung, J.H., Fu, X., Yang, P.C., 2017. Exosomes generated from iPSC-derivatives: New direction for stem cell therapy in human heart diseases. Circ. Res. 120, 407–417. https://doi.org/10.1161/CIRCRESAHA.116.309307.
Jurgielewicz, B.J., Yao, Y., Stice, S.L., 2020. Kinetics and specificity of HEK293T extracellular vesicle uptake using imaging flow cytometry. Nanoscale Res. Lett. 15, 170. https://doi.org/10.1186/s11671-020-03399-6.
Kalluri, R., LeBleu, V.S., 2020. The biology function, and biomedical applications of exosomes. Science 367, eaau6977. https://doi.org/10.1126/science.aau6977.
Katzmann, D.J., Babst, M., Emr, S.D., 2001. Ubiquitin-dependent sorting into the multivesicular body pathway requires the function of a conserved endosomal protein sorting complex, ESCRT-I. Cell 106, 145–155. https://doi.org/10.1016/s0092-8674(01)00434-2.
Kharkar, P.M., Kiick, K.L., Kloxin, A.M., 2013. Designing degradable hydrogels for orthogonal control of cell microenvironments. Chem. Soc. Rev. 42, 7335–7372. https://doi.org/10.1039/C3CS60040H.
Kobayashi, T., Chanmee, T., Itano, N., 2020. Hyaluronan: Metabolism and function. Biomolecules 10, 1525. https://doi.org/10.3390/biom10111525.
Lai, C.P., Mardini, O., Ericsson, M., Prabhakar, S., Maguire, C.A., Chen, J.W., Tannous, B. A., Breakefield, X.O., 2014. Dynamic biodistribution of extracellular vesicles in vivo using a multimodal imaging reporter. ACS Nano 8, 483–494. https://doi.org/10.1021/nn404945r.
Lässer, C., Eldh, M., Lötvall, J., 2012. Isolation and characterization of RNA-containing exosomes. J. Vis. Exp. 3037. https://doi.org/10.3791/3037.
Lee, F., Chung, J.E., Kurisawa, M., 2009. An injectable hyaluronic acid–tyramine hydrogel system for protein delivery. J. Control. Release 134, 186–193. https://doi.org/10.1016/j.jconrel.2008.11.028.
Lee, J.H., 2018. Injectable hydrogels delivering therapeutic agents for disease treatment and tissue engineering. Biomater. Res. 22, 27. https://doi.org/10.1186/s40824-018-0138-6.
Li, J., Chen, X., Yi, J., Liu, Y., Li, D., Wang, J., Hou, D., Jiang, X., Zhang, J., Wang, J., 2016. Identification and characterization of 293T cell-derived exosomes by profiling the protein, mRNA and microRNA components. PLoS One 11, e0163043. https://doi.org/10.1371/journal.pone.0163043.
Li, J., Mooney, D.J., 2016. Designing hydrogels for controlled drug delivery. Nat. Rev. Mater. 1, 16071. https://doi.org/10.1038/natrevmats.2016.71.
Lu, M., Xing, H., Xun, Z., Yang, T., Ding, P., Cai, C., Wang, D., Zhao, X., 2018. Exosome-based small RNA delivery: Progress and prospects. Asian J. Pharm. Sci. 13, 1–11. https://doi.org/10.1016/j.ajps.2017.07.008.
Ma, Y., Brocchini, S., Williams, G.R., 2023. Extracellular vesicle-embedded materials. J. Control. Release 361, 280–296. https://doi.org/10.1016/j.jconrel.2023.07.059.
Ma, Y., Yu, Z., Waudby, C.A., Ju, T., Zhou, X., Brocchini, S., Williams, G.R., 2025. Development of hyaluronic acid/β-cyclodextrin semi-interpenetrating network hydrogels for prolonged delivery of water-soluble sunitinib malate. Int. J. Pharm. 669, 125039. https://doi.org/10.1016/j.ijpharm.2024.125039.
Maroto, R., Zhao, Y., Jamaluddin, M., Popov, V.L., Wang, H., Kalubowilage, M., Zhang, Y., Luisi, J., Sun, H., Culbertson, C.T., Bossmann, S.H., Motamedi, M., Brasier, A.R., 2017. Effects of storage temperature on airway exosome integrity for diagnostic and functional analyses. J. Extracell. Ves. 6, 1359478. https://doi.org/10.1080/20013078.2017.1359478.
Melling, G.E., Carollo, E., Conlon, R., Simpson, J.C., Carter, D.R.F., 2019. The challenges and possibilities of extracellular vesicles as therapeutic vehicles. Eur. J. Pharm. Biopharm. 144, 50–56. https://doi.org/10.1016/j.ejpb.2019.08.009.
Pegtel, D.M., Gould, S.J., 2019. Exosomes. Annu. Rev. Biochem. 88, 487–514. https://doi.org/10.1146/annurev-biochem-013118-111902.
Rackov, G., Garcia-Romero, N., Esteban-Rubio, S., Carrión-Navarro, J., Belda-Iniesta, C., Ayuso-Sacido, A., 2018. Vesicle-mediated control of cell function: The role of extracellular matrix and microenvironment. Front. Physiol. 9, 651. https://doi.org/10.3389/fphys.2018.00651.
Rah, M.J., 2011. A review of hyaluronan and its ophthalmic applications. Optomet. – J. Am. Optomet. Assoc. 82, 38–43. https://doi.org/10.1016/j.optm.2010.08.003.
Riau, A.K., Ong, H.S., Yam, G.H.F., Mehta, J.S., 2019. Sustained delivery system for stem cell-derived exosomes. Front. Pharmacol. 10, 1368. https://doi.org/10.3389/fphar.2019.01368.
Saranraj, P., Naidu, M.A., 2013. Hyaluronic acid production and its applications-a review. Int. J. Pharm. Biol. Arch. 4, 853–889.
Simons, M., Raposo, G., 2009. Exosomes–vesicular carriers for intercellular communication. Curr. Opin. Cell Biol. 21, 575–581. https://doi.org/10.1016/j.ceb.2009.03.007.
Sivanantham, A., Jin, Y., 2022. Impact of storage conditions on EV integrity/surface markers and cargos. Life 12, 697. https://doi.org/10.3390/life12050697.
Stocke, N.A., Zhang, X., Hilt, J.Z., DeRouchey, J.E., 2017. Transport in PEG-based hydrogels: Role of water content at synthesis and crosslinker molecular weight. Macro Chemistry & Physics 218, 1600340. https://doi.org/10.1002/macp.201600340.
Strand, V., Baraf, H.S., Lavin, P.T., Lim, S., Hosokawa, H., 2012. A multicenter, randomized controlled trial comparing a single intra-articular injection of Gel-200, a new cross-linked formulation of hyaluronic acid, to phosphate buffered saline for treatment of osteoarthritis of the knee. Osteoarthr. Cartil. 20, 350–356. https://doi.org/10.1016/j.joca.2012.01.013.
Su, J., Hu, B.H., Lowe Jr, W.L., Kaufman, D.B., Messersmith, P.B., 2010. Anti-inflammatory peptide-functionalized hydrogels for insulin-secreting cell encapsulation. Biomaterials 31, 308–314. https://doi.org/10.1016/j.biomaterials.2009.09.045.
Takahashi, Y., Nishikawa, M., Shinotsuka, H., Matsui, Y., Ohara, S., Imai, T., Takakura, Y., 2013. Visualization and in vivo tracking of the exosomes of murine melanoma B16-BL6 cells in mice after intravenous injection. J. Biotechnol. 165, 77–84. https://doi.org/10.1016/j.jbiotec.2013.03.013.
Théry, C., Witwer, K.W., Aikawa, E., et al., 2018. Minimal information for studies of extracellular vesicles 2018 (MISEV2018): A position statement of the International Society for Extracellular Vesicles and update of the MISEV2014 guidelines. J. Extracell. Ves. 7, 1535750. https://doi.org/10.1080/20013078.2018.1535750.
Toh, W.S., Lim, T.C., Kurisawa, M., Spector, M., 2012. Modulation of mesenchymal stem cell chondrogenesis in a tunable hyaluronic acid hydrogel microenvironment. Biomaterials 33, 3835–3845. https://doi.org/10.1016/j.biomaterials.2012.01.065.

Uppal, R., Ramaswamy, G.N., Arnold, C., Goodband, R., Wang, Y., 2011. Hyaluronic acid nanofiber wound dressing—production, characterization, and in vivo behavior. J Biomed Mater Res 97B, 20–29. https://doi.org/10.1002/jbm.b.31776.

Valadi, H., Ekström, K., Bossios, A., Sjöstrand, M., Lee, J.J., Lötvall, J.O., 2007. Exosome-mediated transfer of mRNAs and microRNAs is a novel mechanism of genetic exchange between cells. Nat. Cell Biol. 9, 654–659. https://doi.org/10.1038/ncb1596.

Webber, J., Clayton, A., 2013. How pure are your vesicles? J. Extracell. Ves. 2, 19861. https://doi.org/10.3402/jev.v2i0.19861.

Wiklander, O.P.B., Nordin, J.Z., O'Loughlin, A., Gustafsson, Y., Corso, G., Mäger, I., Vader, P., Lee, Y., Sork, H., Seow, Y., Heldring, N., Alvarez-Erviti, L., Smith, C.E., Le Blanc, K., Macchiarini, P., Jungebluth, P., Wood, M.J.A., Andaloussi, S.E., 2015. Extracellular vesicle in vivo biodistribution is determined by cell source, route of administration and targeting. J. Extracell. Ves. 4, 26316. https://doi.org/10.3402/jev.v4.26316.

Wu, K., He, C., Wu, Y., Zhou, X., Liu, P., Tang, W., Yu, M., Tian, W., 2021. Preservation of small extracellular vesicle in gelatin methacryloyl hydrogel through reduced particles aggregation for therapeutic applications. IJN 16, 7831–7846. https://doi.org/10.2147/IJN.S334194.

Yasin, A., Ren, Y., Li, J., Sheng, Y., Cao, C., Zhang, K., 2022. Advances in hyaluronic acid for biomedical applications. Front. Bioeng. Biotechnol. 10, 910290. https://doi.org/10.3389/fbioe.2022.910290.